MOX-Report No. 42/2024

Landslide run-out simulations with depth-averaged models and integration with 3D impact analysis using the Material Point Method

Fois, M.; Katili M. A.; de Falco C.; Larese A.; Formaggia L.

MOX, Dipartimento di Matematica
Politecnico di Milano, Via Bonardi 9 - 20133 Milano (Italy)

mox-dmat@polimi.it https://mox.polimi.it

Landslide run-out simulations with depth-averaged models and integration with 3D impact analysis using the Material Point Method

Marco Fois [1] Andi Makarim Katili [2] Carlo de Falco[1]
Antonia Larese [3] Luca Formaggia[1]

June 7, 2024

[1] MOX – Modelling and Scientific Computing
Dipartimento di Matematica, Politecnico di Milano
Piazza Leonardo da Vinci, 20133 Milano, Italy
marco.fois@polimi.it
carlo.defalco@polimi.it
luca.formaggia@polimi.it
[2] Department of Structural Analysis, Technical University of Munich
Arcisstr. 21, D-80333 Munich, Germany
andi.katili@tum.de
[3] Department of Mathematics, University of Padua
Via Trieste, 63 - 35121 Padua, Italy
antonia.larese@unipd.it

Keywords: Shallow water, MPM, Depth-Averaged MPM, Landslides, Impact analysis.

AMS Subject Classification: 35Q35, 35L65, 35Q70, 65Z05, 76D05, 76D99

Abstract

Landslides pose a significant threat to human safety and the well-being of communities, making them one of the most challenging natural phenomena. Their potential for catastrophic consequences, both in terms of human lives and economic impact, is a major concern. Additionally, their inherent unpredictability adds to the complexity of managing the risks associated with landslides. It is crucial to continuously monitor areas susceptible to landslides. In situ detection systems like piezometers and strain gauges play a vital role in accurately monitoring internal pressures and surface movements in the targeted areas. Simultaneously, satellite surveys contribute by offering detailed topographic and elevation data for the study area. However, relying solely on empirical monitoring is insufficient for ensuring effective management of hazardous situations, especially in terms of preventive measures. This study provides advanced simulations of mudflows and fast landslides using particle depth-averaged methods, specifically employing the Material Point Method adapted for shallow water (Depth Averaged Material Point Method). The numerical method has been parallelized and validated through benchmark tests and real-world cases. Furthermore, the investigation extends to coupling the depth-averaged formulation with a three-dimensional one in order to have a detailed description of the impact phase of the sliding material on barriers and membranes. The multidimensional approach and its validation on real cases provide a robust foundation for a more profound and accurate understanding of the behavior of mudflows and fast landslides.

1 Introduction

The complex phenomenology of landslides manifests across multiple stages. From the initiation phase characterized by intermittent slides influenced by gravity, hydrodynamic soil conditions, and pore pressure, to the run-out phase dominated by viscoplastic behavior and advection [1, 2, 3]. In scenarios such as debris flows or mudslides, the run-out phase exhibits fluid-like characteristics with sustained horizontal speeds. The fundamental mathematical model employed for describing gravity-driven free surface flows encompasses a set of two-dimensional equations derived from the Navier-Stokes equation, integrated in the vertical direction. In this work we focus on the application of a semi-conservative variant of the depth-averaged material point method (DAMPM), an extension of the Material Point Method (MPM) originally stemming from the Particle In Cell (PIC) method [4, 5] in the context of depth-averaged physical models. The appeal of the DAMPM lies in its adaptability to novel parallel computing architectures [6, 7, 8], particularly advantageous for simulating large-area phenomena cost-effectively [3]. Another advantage of using depth-averaged methods for simulating landslide run-out is the utilization of computationally less demanding domains compared to traditional 3D frameworks. This enables the simulation of scenarios that are topologically and rheologically much more complex. Another key point of this work is to show a simple technique of coupling depth-averaged and full 3D models, in MPM context, for impact scenario analysis. The paper is organized as follows. Section 2 is devoted to the governing equations with rheological and constitutive model. We briefly present the (DA)MPM framework in Section 3 and the coupling technique we adopted in Section 4. Finally we present some numerical results and draw some conclusions in Section 5 and Section 6 respectively.

2 Physical model

According to the works presented in [3, 9, 10], flow-like landslides and mudflows can be represented using a series of equations derived from the depth-integrated Navier-Stokes

equations, assuming a hydrostatic pressure distribution along the vertical axis. This approach is based on the assumption that the vertical scale of the moving material is significantly smaller than the horizontal counterpart. In this context, we consider a domain $\Omega \subset \mathbb{R}^2$ and the time interval $(0, T]$ with $T > 0$. We take the conservative form of the depth-averaged equations for the unknown elevation h and linear momenta $h\mathbf{v}$, given by

$$\begin{cases} \partial_t h + \nabla \cdot (h\mathbf{v}) = 0, \\ \partial_t (h\mathbf{v}) + \nabla \cdot \left(\mathbf{v} \otimes h\mathbf{v} + \frac{1}{2} g h^2 \otimes \mathbb{I} \right) = \frac{1}{\rho} \nabla \cdot (h\boldsymbol{\sigma}) + \frac{1}{\rho} \mathbf{B}^f - gh \nabla Z, \end{cases} \tag{1}$$

where $\mathbf{v} = [u, v]^T$ is the horizontal velocity vector, g the gravitational acceleration, ρ the density of the material, assumed constant, $\mathbf{B}^f = [B_x, B_y]^T$ the bed friction, $Z = Z(x, y)$ the orography, $\boldsymbol{\sigma} = [\sigma_{xx}, \sigma_{yy}, \sigma_{xy}]$ the deviatoric part of the Cauchy stress tensor and $\mathbb{I}$ is the identity tensor.

2.1 Rheological and constitutive model

The integration of both turbulent and frictional models is warranted by the characteristics of the phenomena being studied, and it has been shown that this approach produces favorable results for velocity and deposition in simulations [11, 12, 13]. Accordingly, in the right-hand side of equation (1), we have included a bed friction term $\mathbf{B}^f$ as described by the Voellmy model, defined as follows:

$$\mathbf{B}^f = - \left(p^A \tan \varphi + \rho g h \tan \varphi + \frac{\rho g |\mathbf{v}|^2}{\xi} \right) \frac{\mathbf{v}}{|\mathbf{v}|}, \tag{2}$$

where φ represents the friction angle, p^A the atmospheric pressure and ξ the turbulence coefficient. Regarding the constitutive law, we adopted a depth-integrated variant of the Bingham rheological model for visco-plastic materials, by defining the Cauchy stress tensor $\boldsymbol{\sigma}$ as

$$\boldsymbol{\sigma} = \left(2\mu + \frac{\tau_Y}{\mathcal{I}_2} \right) \mathbf{D}. \tag{3}$$

where μ is the material viscosity, τ_Y the yield shear stress, $\mathbf{D}$ represents the strain rate tensor defined by

$$\mathbf{D} = \begin{bmatrix} \partial_x u & \frac{1}{2}(\partial_y u + \partial_x v) \\ \frac{1}{2}(\partial_x u + \partial_y v) & \partial_y v \end{bmatrix}, \tag{4}$$

and $\mathcal{I}_2$ is the second invariant of the depth-averaged strain rate tensor. The reader interested in a deeper discussion can refer to [3].

3 Numerical framework

The system shown in (1) is discretized and solved using a semi-conservative variant of the Depth-Averaged Material Point Method (MPM) [14, 15, 16]. The MPM algorithm operates by representing a continuum material, i.e. the landslide in our study, using a set Ω_p of N_p discrete material points, also known as particles, which are intended as columns in the depth-averaged context, while defining a computational background grid that covers the entire domain Ω. Each particle p is defined by essential physical properties, such as mass m_p, volume V_p, position $\mathbf{x}_p$, velocity $\mathbf{v}_p$, acceleration $\mathbf{a}_p$, stress $\boldsymbol{\sigma}_p$ and height h_p, for every $p \in \{1, ..., N_p\}$ according to the adopted rheological and constitutive model.

The main idea of MPM is to transfer information between the particles p and the nodes $i \in \{1, ..., N_v\}$ of the background grid, on which are defined piecewise bilinear shape functions $N_i(\mathbf{x})$, $\mathbf{x} \in \Omega$, to facilitate the computation of forces and update the material state over time. The computational cycle consists of three main stages, summarized in

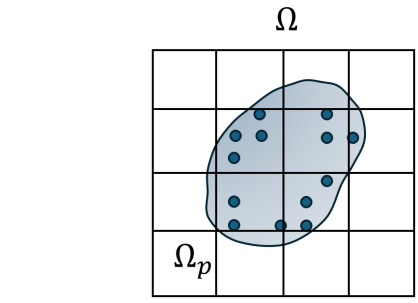

(a) An Eulerian grid is defined in the domain Ω, while the continuous material is discretized into a set Ω_p consisting of N_p Lagrangian points, each possessing distinct physical properties.

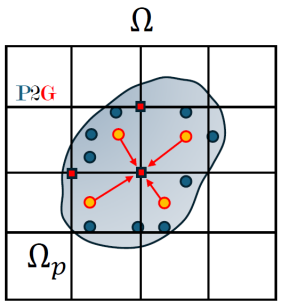

(b) The P2G process involves projecting the physical quantities defined on the particles onto the grid nodes. This is done using the basis functions $N_i(\mathbf{x}_p)$ to assemble the nodal forces $\mathbf{f}_i$.

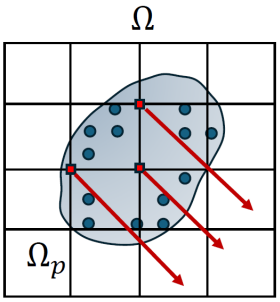

(c) Advective phase on the grid nodes. The nodal accelerations $\mathbf{a}_i$ and velocities $\mathbf{v}_i$, shown here with red arrows, are calculated using the nodal momenta $(m\mathbf{v})_i$ and the total nodal force $\mathbf{f}_i$.

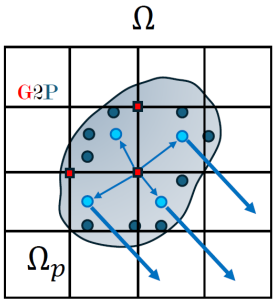

(d) The G2P procedure. The advective phase is projected back to the particles.

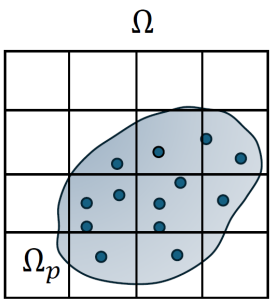

(e) Final stage of the method. After the stresses $\boldsymbol{\sigma}_p$ are calculated, the particle positions $\mathbf{x}_p$ and the depth h_p are updated, and the scheme can be restarted.

Figure 1: Illustration of the classic MPM algorithm.

.

Figure 1: (i) initialization and P2G projection, (ii) advection and (iii) G2P phase. During the initialization and P2G phase, shown in Figure 1(a-b), data is transferred from the material points p to the grid nodes i, by using the shape functions N_i evaluated on the particle position $\mathbf{x}_p$, to collect the nodal internal and external forces $\mathbf{f}_i$. In the advective phase, shown in Figure 1(c) the balance equations are solved on the grid in order to obtain nodal accelerations $\mathbf{a}_i$ and velocities $\mathbf{v}_i$. Finally, the material points are updated with new properties during the G2P phase, in which the quantities just computed on the nodes i are projected back to the particles p, by using the same shape functions N_i as shown in Figure 1(d-e) and the cycle can be started again. Due to space limitations, the specific details of the discretization of the governing equations and the numerical implementation are not included here. Interested readers can refer to [4, 5, 14, 17] for a detailed discussion.

4 Multiscale approach

The coupling between depth-averaged and 3D models is advantageous for two primary reasons. First, it significantly reduces the computational cost, which would be prohibitive if a full 3D simulation were employed for the entire run-out process. Second, it allows for a detailed analysis of the impact phase when the sliding material interacts with barriers and membranes, which would be overly coarse and imprecise if modeled using only a depth-averaged approach. The adopted approach, shown in Figure 2, is straightforward and naive. Initially, the run-out simulation is conducted using a depth-averaged formulation [18]. The duration of this simulation is strictly dependent on the velocities, extents, physical conditions, and other relevant characteristics of the phenomenon under consideration. When the interface of the sliding material reaches a point sufficiently close to the barrier—typically within 10 to 20 meters—a conversion algorithm is applied. At the moment of conversion, an input file is generated containing topological information about the intersection of the domain between the 2D and 3D models, as well as all the physical characteristics of the considered material. This algorithm discretizes each column from the depth-averaged model into an arbitrary, but prefixed, sequence of 3D points. It transfers each property of the column to the newly created particles, ensuring the conservation of mass, volume, and velocity during the conversion.

This method allows for the efficient use of computational resources during the bulk of the simulation while providing the necessary detail for analyzing interactions with barriers and membranes near the point of impact [19].

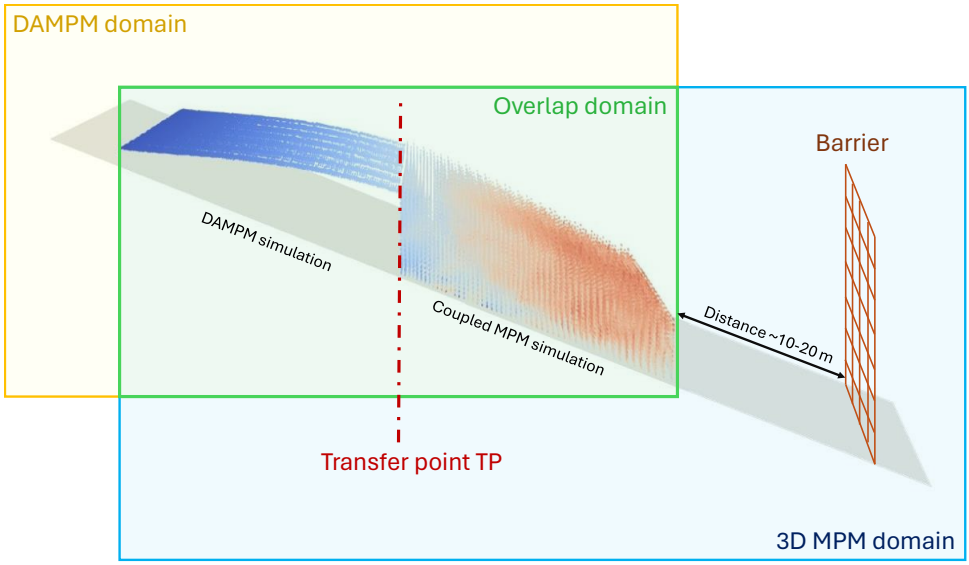

Figure 2: Conversion from DAMPM to 3D MPM.

5 Numerical simulations

This Section is devoted to some numerical results, in which we analyse both idealized and realistic settings.

5.1 Collapse of a semisphere

The first test we carried out deals with the collapse of a semisphere of water under its own weight on a flat, frictionless domain Ω defined by the square $[0, 50]^2$. The initial conditions on the material are set as

$$\begin{aligned} h(\mathbf{x}, 0) &= \sqrt{25 - \|\mathbf{x}\|^2} \\ u(\mathbf{x}, 0) &= v(\mathbf{x}, 0) = 0 \end{aligned}, \qquad \|\mathbf{x}\| \leq 5. \tag{5}$$

The final time is fixed to $T = 1.2\,s$ and non-reflective boundary conditions are enforced at $\partial\Omega$. The simulation with DAMPM model started until the time step $T = 0.65\,s$ is reached, with a number of particles equals to $4.9 \cdot 10^4$. The conversion to the 3D model is applied after $T = 0.65\,s$ by generating $5.1 \cdot 10^5$ particles as shown in Figure 3. The coupled simulation is then carried out for other $0.55\,s$, in order to reach the total time $T = 1.2\,s$.

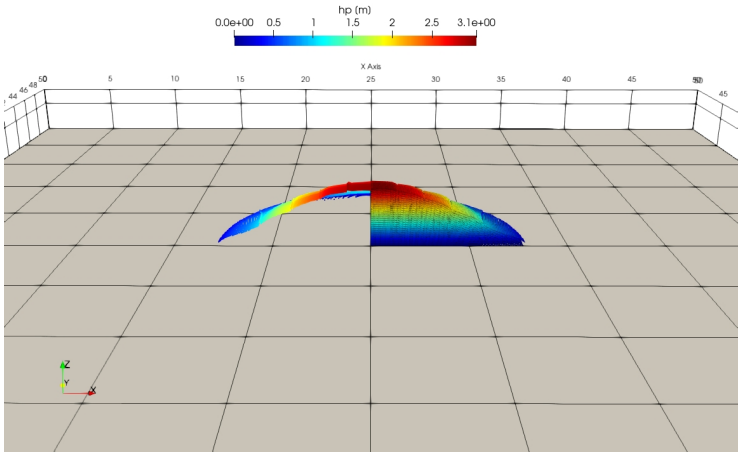

Figure 3: Snapshot of the conversion between DAMPM and 3D MPM after $T = 0.65\,s$ of simulation along the section given by the line $y = 25$.

On the left panel of Figure 4 is depicted a snapshot at the final time step of the Coupled MPM simulation with highlighted velocities, which are consistently symmetrical with respect to the center of the sphere. On the right one, a transversal section of the material, along the line $y = 25$, is shown and juxtaposed to the DAMPM profile of the mass. The error generated on masses and volumes conservation during the conversion from DAMPM to the 3D model has been computed in L^∞ norm and it was not superior to 0.3% and 0.4% respectively. A comparison between the final states of both DAMPM and Coupled simulation, shows an a difference of roughly 12% with respect to the height h of the mass, and about 0.02% with respect to the horizontal extension in x and y directions.

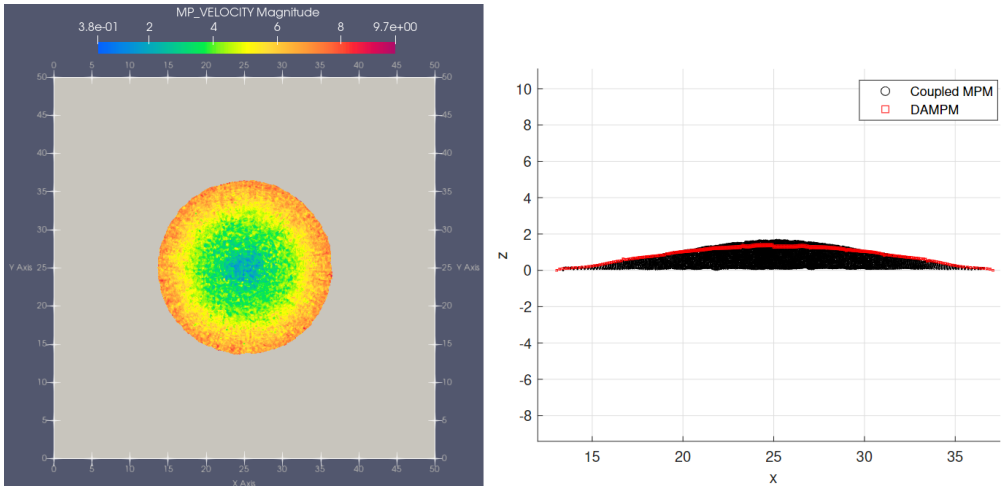

Figure 4: On the left, a snapshot of the Coupled MPM simulation at $T = 1.2\,s$. On the right, the profile of the DAMPM and Coupled MPM simulation at time $T = 1.2\,s$ along the line $y = 25\,m$.

5.2 Sliding to the wall

The second test we carried out deals with a dam break of a water column along a domain $\Omega = [0, 25] \times [0, 5]$ described by the topography

$$Z(\mathbf{x}) = \begin{cases} 10 - \frac{1}{3}x & \text{if } \mathbf{x} \in [0, 10] \times [0, 5] \\ 6.67 & \text{otherwise} \end{cases}. \tag{6}$$

The initial conditions on height h and velocities u, v of the sliding material are prescribed as

$$h(\mathbf{x}, 0) = \begin{cases} 9.5 - Z(\mathbf{x}) & \text{if } \mathbf{x} \in [1.5, 5] \times [0, 5] \\ 0 & \text{otherwise} \end{cases}, \tag{7}$$
$$u(\mathbf{x}, 0) = v(\mathbf{x}, 0) = 0, \quad \forall x \in \boldsymbol{\Omega}.$$

In Figure 5 are depicted the final moments preceding the impact of the water column against a wall located at $x = 20$, after the conversion from the depth-averaged model to the Coupled model made at time $T = 3\,s$. The simulation using the DAMPM was carried out by using $7 \cdot 10^4$ particles, and upon conversion to the 3D model, $5.03 \cdot 10^5$ particles were generated. As shown in Figure 5, the water mass at time $T = 3\,s$ exhibits a constant velocity of approximately $6.8\,m/s$, which aligns with theoretical expectations derived from motion along an inclined plane of about 18° with respect to the horizontal line, followed by motion on a frictionless flat domain. After the impact, occurring at time $T = 3.3\,s$, the water front surges, generating velocity peaks exceeding $20\,m/s$ and surpassing the barrier, reaching a height of nearly $10\,m$.

5.3 A realistic scenario

In the last test we considered a realistic scenario, utilizing a topography derived from a satellite-based digital terrain model (DTM). The qualitative behavior of a mudflow impacting a rigid barrier placed along the path of the moving mass was investigated. The zone of interest is located on a hill in the north part of Italy, near Lecco (LC). In this context, the sliding material occupied an initial volume of about $5.8 \cdot 10^3\,m^3$ with a density

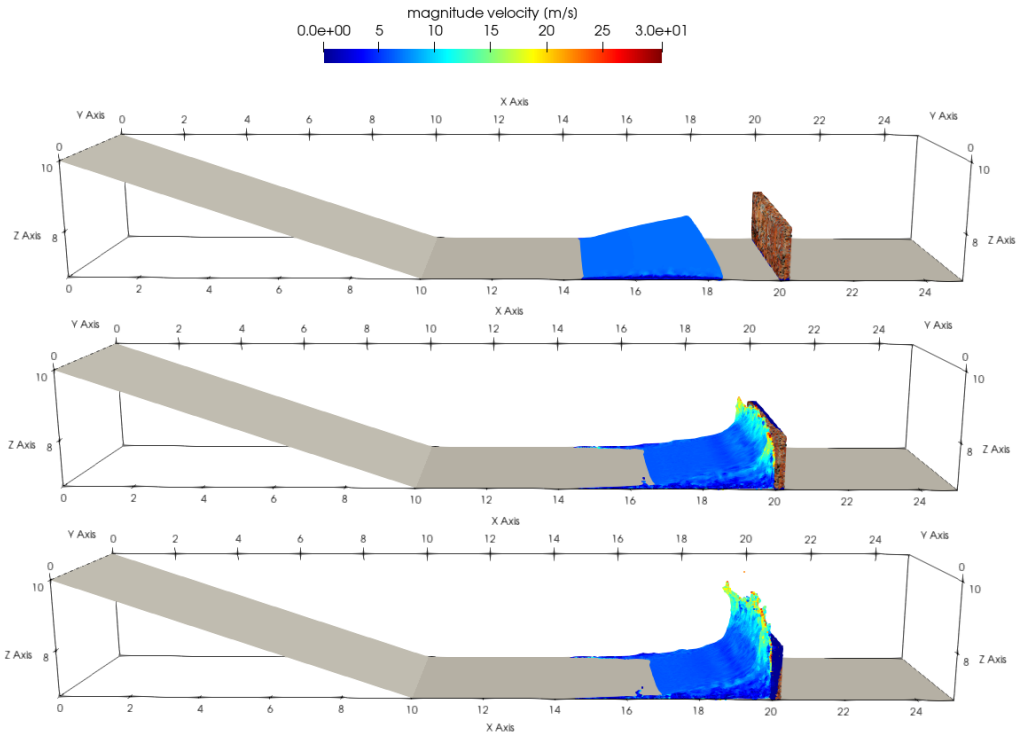

Figure 5: Snapshots of three different time steps of the Coupled MPM, at $T = 3\,s$ (on the top panel), $T = 3.3\,s$ (central panel) and $T = 3.5\,s$ (bottom panel).

ρ equals to $1300\,kg/m^3$. The rheology adopted in this test followed the Voellmy model. The parameters related to the turbulence coefficient, ξ, and the friction angle, ϕ, have been set to $200\,\mathrm{m/s^2}$ and $20°$ respectively. The stress tensor has been defined following the Bingham model, as described in section 2.1, considering a viscosity $\mu = 50\,\mathrm{Pa}$ and a yield shear stress $\tau_Y = 2000\,\mathrm{Pa}\cdot\mathrm{s}$. The final simulation time is set to $T = 38\,\mathrm{s}$. From a numerical point of view, the simulation was carried out using the DAMPM method for the first 30 s, while the remaining 8 s were simulated using the Coupled MPM model. For the depth-averaged simulation, $7.0 \cdot 10^4$ particles were employed, while the conversion to 3D generated $5.6 \cdot 10^5$ particles. Additionally, a rigid L-shaped barrier was placed at the base of the hill, as shown in Figure 6. This barrier, measuring 20 meters in height and 100 meters in length, was designed to contain the sliding mass.
Figure 6 shows different time steps of the front advancement following the conversion to the coupled model. Specifically, the instances shown are at $T = 30\,s$, $T = 34\,s$ and $T = 38\,s$. Although the front advancement speed was sustained and was estimated to be around $20\,m/s$ in the moments just before the impact, the presence of the barrier prevented the landslide mass from reaching the flat areas at the base of the hill. Figure 7 shows the final stage of the event at the instant $T = 38\,s$ in the absence of the barrier. It can be seen how the area previously protected by the barrier is now overtaken by the landslide mass, which is free to proceed towards the surrounding areas and residential centers.

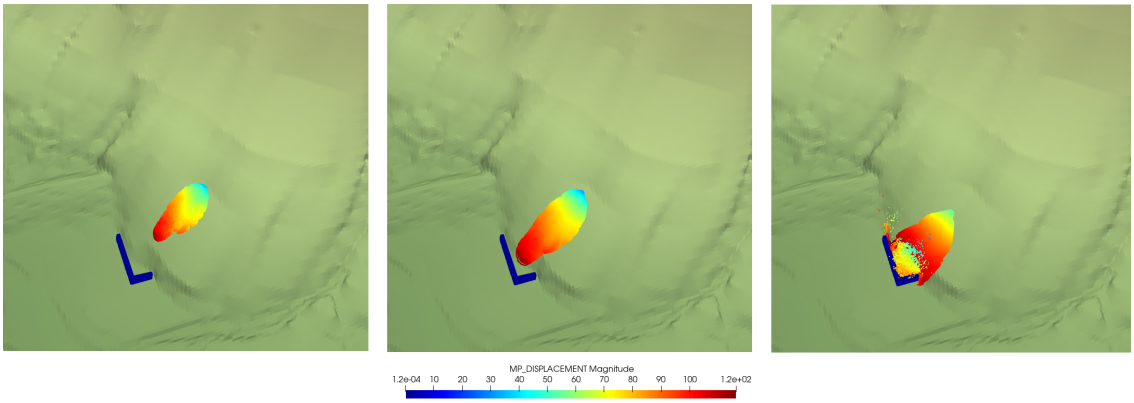

Figure 6: Snapshots of three different time steps of the Coupled MPM, at $T = 30\,s$ (left panel), $T = 33\,s$ (central panel) and $T = 38\,s$ (right panel).

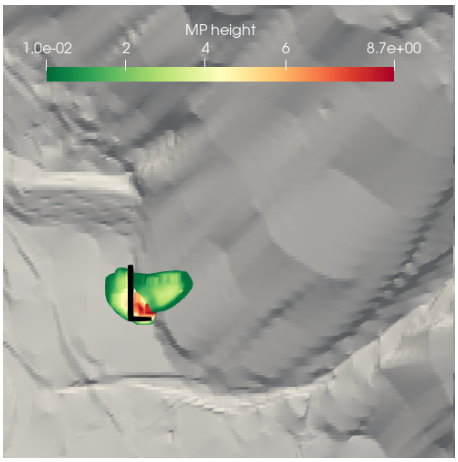

Figure 7: Final state of the landslide in absence of the barrier, here reported just for comparison in black.

6 Conclusions

The presented work focused on coupling techniques between particle-based numerical models for depth-averaged landslide run-out and 3D models. The extremely simple approach allowed for a qualitative exploration of the behavior of landslide masses in collision with obstacles and barriers. The numerical advantage of the multiscale technique lies in having an extremely efficient solver for the run-out phase, thanks to the depth-averaged (2D) formulation, while simultaneously providing a detailed analysis of the impact phase, which can only be achieved with 3D models. However, it should be clarified that the tests conducted and the results obtained must be considered qualitative and partial, although they are consistently aligned with expected or theoretical data.

Acknowledgements

M.F., C.d.F. and L.F. were supported by the Accordo Attuativo ASI-POLIMI “Attività di Ricerca e Innovazione” n. 2018-5-HH.0. C.d.F. and L.F. also acknowledge the support of “Dipartimento di Eccellenza 2023-2027”. C.d.F. and L.F. have been partially funded

by the Italian Research Center on High-Performance Computing, Big Data and Quantum Computing (ICSC), European Union - Next Generation EU.

This study received funding from the European Union - Next Generation EU National Recovery and Resilience Plan [NRRP], Mission 4, Component 2, Investment 1.3–D.D. 1243 2/8/2022, PE0000005 Extended Partnership "RETURN : Multi- Risk sciEnce for resilienT commUnities underR a changiNg climate" and Mission 4, Component 2, Investment 1.5 - Call for tender No. 3277 of 30 dicembre 2021 ECS00000043, No. 1058 of June 23, 2023, CUP C43C22000340006, "iNEST: Interconnected Nord-Est Innovation Ecosystem, and PRIN2022- HYDROROM 2022PXYYK5 - Reduced order models of hydraulic protection systems for extreme water hazards

References

[1] U. Haque, P. F. Da Silva, G. Devoli, J. Pilz, B. Zhao, A. Khaloua, W. Wilopo, P. Andersen, P. Lu, J. Lee, et al., The human cost of global warming: Deadly landslides and their triggers (1995–2014), Science of the Total Environment 682 (2019) 673–684.

[2] U. Haque, P. Blum, P. F. Da Silva, P. Andersen, J. Pilz, S. R. Chalov, J.-P. Malet, M. J. Auflič, N. Andres, E. Poyiadji, et al., Fatal landslides in europe, Landslides 13 (6) (2016) 1545–1554.

[3] F. Gatti, M. Fois, C. de Falco, S. Perotto, L. Formaggia, Parallel simulations for fast-moving landslides: Space-time mesh adaptation and sharp tracking of the wetting front, Int J Numer Meth Fluids 95 (8) (2023) 1286–1309. doi:https://doi.org/10.1002/fld.5186.

[4] D. Sulsky, Z. Chen, H. Schreyer, A particle method for history-dependent materials, Computer Methods in Applied Mechanics and Engineering 118 (1993) 179–196.

[5] D. Sulsky, Erratum: Application of a particle-in-cell method to solid mechanics, Computer Physics Communications (1995).

[6] X. Wang, Y. Qiu, S. R. Slattery, Y. Fang, M. Li, S.-C. Zhu, Y. Zhu, M. Tang, D. Manocha, C. Jiang, A massively parallel and scalable multi-gpu material point method, ACM Trans. Graph. 39 (4) (aug 2020). doi:10.1145/3386569.3392442.
URL `https://doi.org/10.1145/3386569.3392442`

[7] p. Baioni, T. Benacchio, L. Capone, C. de Falco, Gpus based material point method for compressible flows, in: Particles, 2023.
URL `https://www.scipedia.com/public/Baioni_et_al_2023a`

[8] P. J. Baioni, T. Benacchio, L. Capone, C. de Falco, Portable, massively parallel implementation of a material point method for compressible flows, Computational Particle Mechanics (2024).

[9] M. Quecedo, M. Pastor, M. I. Herreros, J. A. Fernández Merodo, Numerical modelling of the propagation of fast landslides using the finite element method, International Journal for Numerical Methods in Engineering 59 (6) (2004) 755–794. doi:https://doi.org/10.1002/nme.841.

[10] M. Pastor, T. Blanc, B. Haddad, V. Drempetic, M. Mories, P. Stickle, M. Mira, J. Merodo, Depth averaged models for fast landslide propagation: mathematical,

rheological and numerical aspects, Archive of Computational Methods in Engineering 22 (2015) 67–104.

[11] M. Mckinnon, O. Hungr, S. McDougall, Dynamic analyses of canadian landslides, Proceedings of the Fourth Canadian Conference on GeoHazards: From Causes to Management (2008) 20–24.

[12] S. Beguería, M. Hees, M. Geertsema, Comparison of three landslide runout models on the turnoff creek rock avalanche, british columbia, in: Landslide Processes Conference: A tribute to Theo van Asch. Strasbourg, 6-7 February, CERG, 2009, pp. 243–247. doi:10.13140/2.1.4569.3767.

[13] R. Sosio, G. Crosta, J. Chen, O. Hungr, Runout prediction of rock avalanches in volcanic and glacial terrains, Landslide Science and Practice: Spatial Analysis and Modelling 3 (2013) 285–291. doi:10.1007/978-3-642-31310-3-38.

[14] M. Fois, C. de Falco, L. Formaggia, A semi-conservative depth-averaged material point method for fast flow-like landslides and mudflows, Tech. Rep. MOX-Report 17/2024 (2024). doi:10.13140/RG.2.2.12510.00322.

[15] L. Guillet, L. Blatny, B. Trottet, D. Steffen, J. Gaume, A depth-averaged material point method for shallow landslides: Applications to snow slab avalanche release, Journal of Geophysical Research: Earth Surface 128 (8) (2023) e2023JF007092, e2023JF007092 2023JF007092. arXiv:https://agupubs.onlinelibrary.wiley.com/doi/pdf/10.1029/2023JF007092, doi:https://doi.org/10.1029/2023JF007092.

[16] K. Abe, K. Konagai, Numerical simulation for runout process of debris flow using depth-averaged material point method, Soils and Foundations 56 (5) (2016) 869–888, special Issue on the International Symposium on Geomechanics from Micro to Macro IS-Cambridge 2014. doi:https://doi.org/10.1016/j.sandf.2016.08.011.

[17] A. de Vaucorbeil, V. P. Nguyen, S. Sinaie, J. Y. Wu, Chapter two - material point method after 25 years: Theory, implementation, and applications, in: S. P. Bordas, D. S. Balint (Eds.), Advances in Applied Mechanics, Vol. 53 of Advances in Applied Mechanics, Elsevier, 2020, pp. 185–398. doi:https://doi.org/10.1016/bs.aams.2019.11.001.

[18] Pasqua, Andrea, Leonardi, Alessandro, Pirulli, Marina, Coupling depth-averaged and 3d numerical models to study debris flow: Saint-vincent event, E3S Web of Conf. 415 (2023) 02015. doi:10.1051/e3sconf/202341502015.
URL `https://doi.org/10.1051/e3sconf/202341502015`

[19] V. Singer, A. Larese, A. Börst, R. Wüchner, K. Bletzinger, Partitioned mpm-fem coupling approach for advanced numerical simulation of massmovement hazards impacting flexible protective structures., 10th edition of the International Conference on Computational Methods for Coupled Problems in Science and Engineering (2023).

MOX Technical Reports, last issues

Dipartimento di Matematica
Politecnico di Milano, Via Bonardi 9 - 20133 Milano (Italy)

41/2024 Bergonzoli, G.; Rossi, L.; Masci, C.
Ordinal Mixed-Effects Random Forest

40/2024 Carrara, D.; Regazzoni, F.; Pagani, S.
Implicit neural field reconstruction on complex shapes from scattered and noisy data

39/2024 Bartsch, J.; Buchwald, S.; Ciaramella, G.; Volkwein, S.
Reconstruction of unknown nonlienar operators in semilinear elliptic models using optimal inputs

38/2024 Tonini, A., Regazzoni, F., Salvador, M., Dede', L., Scrofani, R., Fusini, L., Cogliati, C., Pontone, G., Vergara, C., Quarteroni, A.
Two new calibration techniques of lumped-parameter mathematical models for the cardiovascular system

Fumagalli, A.; Patacchini, F.S.
Numerical validation of an adaptive model for the determination of nonlinear-flow regions in highly heterogeneous porous media

37/2024 Begu, B.; Panzeri, S.; Arnone, E.; Carey, M.; Sangalli, L.M.
A nonparametric penalized likelihood approach to density estimation of space-time point patterns

36/2024 Torri, V.; Ercolanoni, M.; Bortolan, F.; Leoni, O.; Ieva, F.
A NLP-based semi-automatic identification system for delays in follow-up examinations: an Italian case study on clinical referrals

34/2024 Corti, M.
Exploring tau protein and amyloid-beta propagation: a sensitivity analysis of mathematical models based on biological data

35/2024 Botti, L.; Botti, M.; Di Pietro, D.A.; Massa; F.C.
Stability, convergence, and pressure-robustness of numerical schemes for incompressible flows with hybrid velocity and pressure

Corti, M.
Exploring tau protein and amyloid-beta propagation: a sensitivity analysis of mathematical models based on biological data